

Possible antimagnetic rotational band in ^{114}In

Z. H. Zhao (赵子豪),¹ C. B. Li (李聪博),^{2,*} K. Y. Ma (马克岩),^{1,†} X. G. Wu (吴晓光),^{2,‡} Y. Zheng (郑云),² Y. K. Pan (潘禹坤),¹ J. L. Wang (汪金龙),² H. C. Zhang (张会成),¹ Y. C. Hao (郝宜春),¹ X. F. Li (李险峰),¹ G. S. Li (李广生),² S. H. Yao (姚顺和),² C. Y. He (贺创业),² B. B. Yu (于蓓蓓),² X. P. Cao (曹雪朋),^{2,3} S. P. Hu (胡世鹏),^{2,4} J. B. Lu (陆景彬),¹ Y. J. Ma (马英君),¹ D. Yang (杨东),¹ H. D. Wang (王辉东),¹ G. Y. Liu (刘弓冶),¹ L. Li (李黎),¹ C. Xu (徐川),⁵ and Y. Y. Cheng (程奕源)⁵

¹College of Physics, Jilin University, Changchun 130012, China

²China Institute of Atomic Energy, Beijing 102413, China

³Department of Physics, Northeast Normal University, Changchun 130024, China

⁴College of Physics and Technology, Shenzhen University, Shenzhen 518060, China

⁵School of Physics and State Key Laboratory of Nuclear Physics and Technology, Peking University, Beijing 100871, China



(Received 10 January 2023; revised 14 March 2023; accepted 4 April 2023; published 14 April 2023)

High-spin states of ^{114}In were populated using the reaction $^{110}\text{Pd}(^7\text{Li}, 3n)^{114}\text{In}$ at a beam energy of 26 MeV. More than 30 new γ transitions and 20 new levels are identified in ^{114}In . In total, three new bands and a short cascade are observed, among which a new negative-parity $\Delta I = 2$ band built on the $\pi g_{9/2}^{-2}d_{5/2} \otimes \nu h_{11/2}$ configuration before the backbend and the $\pi g_{9/2}^{-2}d_{5/2} \otimes \nu h_{11/2}^3$ configuration after the backbend is established. The properties of this band are discussed based on the classical particle-rotor model calculations. The predicted $B(E2)$ and $\mathfrak{S}^{(2)}/B(E2)$ ratios indicate that the $\Delta I = 2$ band after the backbend, has the characteristics of antimagnetic rotation. Meanwhile, the two-shears-like mechanism for the possible antimagnetic rotational band is examined by investigating the orientation of the angular momenta. A new positive-parity $\Delta I = 1$ band with the configuration of $\pi g_{9/2}^{-1} \otimes \nu(g_{7/2}/d_{5/2})h_{11/2}^2$ is observed.

DOI: 10.1103/PhysRevC.107.044310

I. INTRODUCTION

Antimagnetic rotation (AMR) predicted by Frauendorf in analogy to antiferromagnetism in condensed matter physics is an interesting exotic phenomenon observed in some nearly spherical or weakly deformed nuclei [1]. In AMR bands, the two proton angular momentum vectors are aligned back to back in opposite directions, nearly perpendicular to the total angular momentum vector of the valence neutrons at the bandhead. The angular momentum is increased by the so-called “two-shears-like mechanism”, i.e., by the simultaneous closing of the two protons blades toward the total angular momentum vector. The phenomenon of AMR band is characterized by the appearance of the weak $E2$ transitions reflecting the weakly deformed or nearly spherical core, the decreasing of the $B(E2)$ values with increasing spin, and a large $\mathfrak{S}^{(2)}/B(E2)$ ratio [1].

Experimentally, most of the antimagnetic rotational bands were reported in Pd ($Z = 46$) [2–7], Cd ($Z = 48$) [8–14], and In ($Z = 49$) [15–18] isotopes including $^{99,100,101,102,103,104,105}\text{Pd}$, $^{105,106,107,108,109,110,111}\text{Cd}$ and $^{108,109,110,112,113}\text{In}$ in the $A \approx 110$ mass region. These provide support for the existence of a small ‘island’ of antimagnetic

rotational structures in the $A \approx 110$ mass region. For a deeper understanding of the systematically appearing antimagnetic rotational bands, it is important to try to experimentally define the boundaries of this island where antimagnetic rotational bands appear in this mass region. For this purpose, the odd-odd ^{114}In ($N = 65$, $Z = 49$) nucleus lying at the extremes of both the N and Z ranges, is suggested to be a good case for testing the limits of this region of antimagnetic rotation. Previously, the antimagnetic rotational bands have been reported in neighboring indium isotopes $^{108,109,110,112,113}\text{In}$. It is interesting to investigate the two-shears-like mechanism along an indium isotopic chain moving away from the shell closure coming close to the $N = 66$ neutron midshell. Hence, we try to extend the study of antimagnetic rotation band to relatively neutron-rich ^{114}In nucleus to explore the boundary of the antimagnetic rotational island.

II. EXPERIMENTAL DETAILS

High-spin states of ^{114}In were populated through the $^{110}\text{Pd}(^7\text{Li}, 3n)^{114}\text{In}$ reaction at a beam energy of 26 MeV. The ^{110}Pd target, with a thickness of 2.45 mg/cm², was rolled onto a 10.55 mg/cm² Au backing. The beam was provided by the HI-13 tandem accelerator at CIAE in Beijing. The γ rays were detected with an array consisting of 12 Compton-suppressed HPGe detectors and two planar-type HPGe detectors. Five of these detectors were placed at 90°, three at 150°, two each at 42° and 140°, and one each at

*licb@ciae.ac.cn

†mky@jlu.edu.cn

‡wxg@ciae.ac.cn

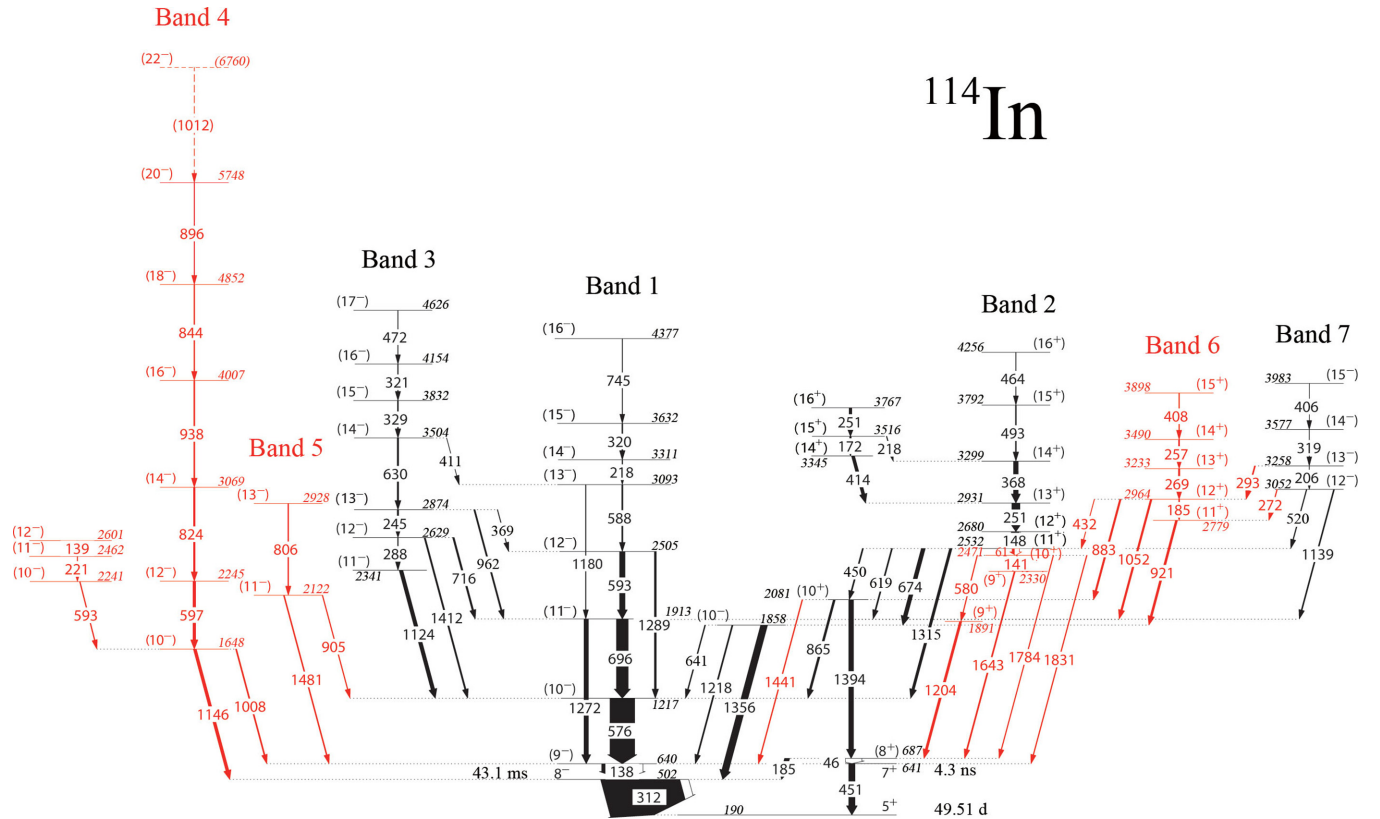


FIG. 1. Partial level scheme of ^{114}In deduced from the present work. Transition energies are given in keV and their measured relative intensities are proportional to the widths of the arrows. New transitions and levels are marked as red.

34° and 127° with respect to the beam direction. A total of 3.5×10^7 γ - γ twofold and higher coincidence events were recorded. The data were sorted into a symmetrized γ - γ coincidence matrix and a directional correlation from oriented states (DCO) matrix [19]. The DCO matrix was created by sorting the detectors at 42° on one axis and the detectors at 90° on the other. The present work is result of further analysis of previous experimental data, and the description of the experimental details has been given in Ref. [20].

III. RESULTS

The level scheme of ^{114}In nucleus derived from the present work, and typical γ -ray coincidence spectra are shown in Figs. 1 and 2, respectively. The majority of transitions of ^{114}In reported in the previous work have been identified [20], but bands 5 and 6 in Ref. [20] are not confirmed in the present work. Because band 6 is from the contaminant of ^{56}Fe , and band 5 is not found any coincidence relationships with other known bands of ^{114}In , bands 5 and 6 in Ref. [20] are not presented in the current paper. In Fig. 1, seven band-like structures are shown and labeled 1–7 for the facility of discussions. Among them, band 2, band 3, and band 7 have been reported in the previous work by Li *et al.* [20]. Band 4, band 5, and band 6 are observed in the present work. The γ -ray energies, excitation energies, relative intensities, DCO ratios, multipolarity, and spin-parity assignments of levels in ^{114}In

extracted from the current work are listed in Table I. The relevant details of the level scheme will be described below.

Band 2 was determined to be a sequence of $\Delta I = 1$ γ transitions in Ref. [20]. In the present study, a new transition of 61 keV are observed and placed at the bottom of band 2 on the basis of the coincidence relationships, intensity balances, and energy sums, and thus the $I^\pi = (10^+)$ level of band 2 is tentatively assigned as the lowest observed state of this band. Moreover, several new linking transitions of 141, 580, 1204, 1643, 1784, and 1831 keV are found between band 2 and low-lying states. The existence of these transitions further strengthens the placements and spin-parity assignments of the levels in band 2. A sample spectrum is provided in Fig. 2(a).

Band 4 is a newly observed band. The new linking transitions of 1008 keV and 1146 keV between bands 1 and 4 are observed. Multipolarity analysis indicates that the 1008 keV linking transition is of $\Delta I = 1$ character with DCO ratio of 1.04 (DCO ratios from gating on the dipole transition), and the 1146 keV linking transition is of $\Delta I = 2$ character with DCO ratio of 1.08 (DCO ratios from gating on the quadrupole transition). The observation of $\Delta I = 1$ and $\Delta I = 2$ linking transitions implies that the spin and parity of the lowest observed state of band 4 is deduced to be $I^\pi = (10^-)$. In the present work, six new intraband transitions of 597, 824, 938, 844, 896, 1012 keV are observed and the ordering of these transitions is deduced based on their relative intensities. Figure 2(b) shows a γ -ray coincidence spectrum generated from the 597 keV transition. Multipolarity analysis indicates that

TABLE I. Energies, excitation energies, relative intensities, DCO ratios, initial and final state spins, and multiplicities for transitions assigned to ^{114}In in the present work.

E_γ^a (keV)	E_i (keV)	I_γ^b	R_{DCO}^c	R_{DCO}^d	$I_i^\pi \rightarrow I_f^\pi$	Multiplicity
45.78 ^e	687				$(8^+) \rightarrow 7^+$	$M1^e$
61.2	2532	6.8(17)			$(11^+) \rightarrow (10^+)$	$(M1 + E2)$
138.4 ^g	640	100.0(7)	1.08(4)		$(9^-) \rightarrow 8^-$	$(M1 + E2)$
139.2	2601	1.4(12)			$(12^-) \rightarrow (11^-)$	$(M1 + E2)$
140.8	2471	2.0(16)	0.91(22)		$(10^+) \rightarrow (9^+)$	$(M1 + E2)$
148.4 ^g	2680	23.3(25)	0.92(15)	0.46(12)	$(12^+) \rightarrow (11^+)$	$(M1 + E2)$
171.6 ^g	3516	4.1(3)	0.99(13)		$(15^+) \rightarrow (14^+)$	$M1 + E2$
185.3 ^f	687	13.9(13) ^f		0.97(8)	$(8^+) \rightarrow 8^-$	$(E1)$
185.6	2964	2.6(10)	0.88(21)		$(12^+) \rightarrow (11^+)$	$(M1 + E2)$
205.7 ^f	3258	<1			$(13^-) \rightarrow (12^-)$	$(M1 + E2)$
217.4 ^g	3516	4.6(6)	1.12(10)		$(15^+) \rightarrow (14^+)$	$(M1 + E2)$
218.3 ^f	3311	<1			$(14^-) \rightarrow (13^-)$	$(M1 + E2)$
221.5	2462	1.7(10)		0.59(15)	$(11^-) \rightarrow (10^-)$	$(M1 + E2)$
245.1 ^g	2874	4.0(2)	0.94(16)	0.63(6)	$(13^-) \rightarrow (12^-)$	$(M1 + E2)$
250.7 ^g	2931	22.4(13)	0.99(10)		$(13^+) \rightarrow (12^+)$	$(M1 + E2)$
251.2 ^g	3767	7.6(18)			$(16^+) \rightarrow (15^+)$	$(M1 + E2)$
257.5	3490	3.0(8)	0.88(21)		$(14^+) \rightarrow (13^+)$	$(M1 + E2)$
268.4	3233	4.1(6)	0.92(19)		$(13^+) \rightarrow (12^+)$	$(M1 + E2)$
272.4	3052	1.9(11)	0.86(12)		$(12^-) \rightarrow (11^+)$	$(E1)$
288.2 ^f	2629	1.7(4) ^f	1.0(8)		$(12^-) \rightarrow (11^-)$	$(M1 + E2)$
293.6	3258	3.1(8)	0.94(10)		$(13^-) \rightarrow (12^+)$	$(E1)$
311.665 ^f	502	224(20) ^f			$8^- \rightarrow 5^+$	$E3^f$
319.0 ^f	3577	<1			$(14^-) \rightarrow (13^-)$	$(M1 + E2)$
320.4 ^f	3632	2.4(9)	0.99(7) ^f		$(15^-) \rightarrow (14^-)$	$(M1 + E2)$
321.3 ^g	4154	2.0(3)	0.96(10)		$(16^-) \rightarrow (15^-)$	$(M1 + E2)$
328.6 ^g	3832	2.6(2)	0.97(22)		$(15^-) \rightarrow (14^-)$	$(M1 + E2)$
368.3 ^g	3299	13.5(7)	1.02(13)	0.61(3)	$(14^+) \rightarrow (13^+)$	$(M1 + E2)$
369.0 ^g	2874	1.3(4)			$(13^-) \rightarrow (12^-)$	$(M1 + E2)$
406.4 ^f	3983	<1			$(15^-) \rightarrow (14^-)$	$(M1 + E2)$
407.3	3898	1.6(8)	1.04(24)		$(15^+) \rightarrow (14^+)$	$(M1 + E2)$
410.7 ^f	3504	<1			$(14^-) \rightarrow (13^-)$	$(M1 + E2)$
414.1 ^g	3345	8.7(6)	1.15(7)	0.59(14)	$(14^+) \rightarrow (13^+)$	$(M1 + E2)$
432.3	2964	1.1(8)			$(12^+) \rightarrow (11^+)$	$(M1 + E2)$
450.6 ^g	2532	3.3(5)			$(11^+) \rightarrow (10^+)$	$(M1 + E2)$
451.1 ^f	641	18.0(10) ^f			$7^+ \rightarrow 5^+$	$E2^f$
464.2 ^f	4256	<1			$(16^+) \rightarrow (15^+)$	$(M1 + E2)$
472.0 ^f	4626	<1			$(17^-) \rightarrow (16^-)$	$(M1 + E2)$
492.6 ^f	3792	2.6(4)	1.0(9)		$(15^+) \rightarrow (14^+)$	$(M1 + E2)$
520.3 ^f	3052	<1			$(12^-) \rightarrow (11^+)$	$(E1)$
576.5 ^f	1217	72.0(11)	1.04(10) ^f		$(10^-) \rightarrow (9^-)$	$(M1 + E2)$
580.2	2471	1.9(6)	1.09(18)		$(10^+) \rightarrow (9^+)$	$(M1 + E2)$
587.8 ^g	3093	3.6(2)	1.07(26)		$(13^-) \rightarrow (12^-)$	$(M1 + E2)$
592.6 ^g	2505	15.6(14)	0.92(8)	0.56(17)	$(12^-) \rightarrow (11^-)$	$(M1 + E2)$
593.4	2241	2.1(13)		1.03(19)	$(10^-) \rightarrow (10^-)$	$(M1 + E2)$
596.9	2245	7.7(4)	1.55(12)	1.14(15)	$(12^-) \rightarrow (10^-)$	$(E2)$
618.9 ^f	2532	3.3(5) ^f		0.97(18)	$(11^+) \rightarrow (11^-)$	$(E1)$
629.5 ^g	3504	4.0(5)	0.87(7)		$(14^-) \rightarrow (13^-)$	$(M1 + E2)$
641.3 ^f	1858	2.5(2) ^f	1.48(20)		$(10^-) \rightarrow (10^-)$	$(M1 + E2)$
673.5 ^g	2532	11.2(2)	0.97(10)	0.51(7)	$(11^+) \rightarrow (10^-)$	$(E1)$
695.9 ^g	1913	34.1(11)	0.95(7)		$(11^-) \rightarrow (10^-)$	$(M1 + E2)$
716.5 ^g	2629	4.6(6)	0.97(18)		$(12^-) \rightarrow (11^-)$	$(M1 + E2)$
744.8 ^f	4377	<1			$(16^-) \rightarrow (15^-)$	$(M1 + E2)$
806.3	2928	2.3(8)		0.98(16)	$(13^-) \rightarrow (11^-)$	$(E2)$
824.5	3069	4.8(4)	1.66(15)	0.87(10)	$(14^-) \rightarrow (12^-)$	$(E2)$
844.5	4852	2.6(6)	1.52(13)	1.12(17)	$(18^-) \rightarrow (16^-)$	$(E2)$
865.4 ^f	2081	5.7(3) ^f	1.56(18)		$(10^+) \rightarrow (10^-)$	$(E1)$

TABLE I. (*Continued.*)

E_γ^a (keV)	E_i (keV)	I_γ^b	R_{DCO}^c	R_{DCO}^d	$I_i^\pi \rightarrow I_f^\pi$	Multipolarity
883.2	2964	4.6(4)		0.95(21)	(12 ⁺) \rightarrow (10 ⁺)	(E2)
895.1	5748	1.6(8)		1.11(17)	(20 ⁻) \rightarrow (18 ⁻)	(E2)
904.6	2122	1.9(7)	0.95(12)		(11 ⁻) \rightarrow (10 ⁻)	(M1 + E2)
921.0	2779	5.8(4)		0.68(20)	(11 ⁺) \rightarrow (10 ⁻)	(E1)
937.6	4007	3.3(7)	1.46(21)	1.07(18)	(16 ⁻) \rightarrow (14 ⁻)	(E2)
961.6 ^g	2874	3.8(5)	1.60(28)		(13 ⁻) \rightarrow (11 ⁻)	(E2)
1007.8	1648	3.2(10)	1.04(17)		(10 ⁻) \rightarrow (9 ⁻)	(M1 + E2)
1012.2	6760	<1			(22 ⁻) \rightarrow (20 ⁻)	(E2)
1051.9	2964	4.8(4)	0.86(16)		(12 ⁺) \rightarrow (11 ⁻)	(E1)
1124.2 ^g	2341	10.4(7)	1.19(19)		(11 ⁻) \rightarrow (10 ⁻)	(M1 + E2)
1139.2 ^g	3052	2.0(5)			(12 ⁻) \rightarrow (11 ⁻)	(M1 + E2)
1146.1	1648	8.3(5)		1.08(15)	(10 ⁻) \rightarrow 8 ⁻	(E2)
1180.4 ^f	3093	1.7(6)			(13 ⁻) \rightarrow (11 ⁻)	(E2)
1203.5	1891	5.2(4)		0.61(12)	(9 ⁺) \rightarrow (8 ⁺)	(M1 + E2)
1217.7 ^g	1858	3.4(5)			(10 ⁻) \rightarrow (9 ⁻)	(M1 + E2)
1272.3 ^g	1913	13.0(5)	1.79(32)		(11 ⁻) \rightarrow (9 ⁻)	(E2)
1288.5 ^g	2505	5.5(4)	1.66(34)		(12 ⁻) \rightarrow (10 ⁻)	(E2)
1314.5 ^g	2532	7.1(2)	0.86(13)		(11 ⁺) \rightarrow (10 ⁻)	(E1)
1356.2 ^g	1858	19.4(3)	1.77(16)		(10 ⁻) \rightarrow 8 ⁻	(E2)
1394.1	2081	13.9(2) ^f		1.04(8) ^f	(10 ⁺) \rightarrow (8 ⁺)	(E2)
1412.4 ^g	2629	4.0(6)	1.67(26)		(12 ⁻) \rightarrow (10 ⁻)	(E2)
1441.3	2081	2.3(2)	1.12(14)		(10 ⁺) \rightarrow (9 ⁻)	(E1)
1481.6	2122	2.7(9)	1.56(17)		(11 ⁻) \rightarrow (9 ⁻)	(E2)
1642.8	2330	3.3(16)			(9 ⁺) \rightarrow (8 ⁺)	(M1 + E2)
1783.2	2471	1.8(11)			(10 ⁺) \rightarrow (8 ⁺)	(E2)
1830.6	2471	2.0(10)			(10 ⁺) \rightarrow (9 ⁻)	(E1)

^aThe uncertainty in strong γ -ray energies is less than 0.3 keV; for weak γ -ray energies, it is about 0.7 keV.

^bIntensities are corrected for detector efficiency and normalized to 100 for the 138 keV transition.

^cThe DCO values are obtained from a gate on the dipole transitions.

^dThe DCO values are obtained from a gate on the quadrupole transitions.

^eData are taken from [21].

^fData are taken from [20].

^g γ -ray energies, relative intensities, DCO ratios, and initial- and final-state spins adopted from previous work [20].

the intraband transitions are consistent with $\Delta I = 2$ character from gating on the quadrupole transitions. To further assist the spin-parity assignment of band 4, the DCO ratios for the members (597, 824, 938, and 844 keV) of band 4 coming from a gate on dipole transition of 138 keV below the band are also presented in Table I. Thus, the spin of band 4 is extended to $I^\pi = (22^-)$. In addition, a short cascade consisting of two weak $\Delta I = 1$ transitions of 139 keV and 221 keV is observed for first time. It decays to band 4 by just a transition of 593 keV. Hence, the firm excitation energies for the short cascade have not been determined.

Band 5 is identified, which decays to the yrast band via two linking transitions with energies of 1481 and 905 keV. Multipolarity analysis indicates that the 1481 and 905 keV linking transitions are of $\Delta I = 2$ and $\Delta I = 1$, respectively. Thus, band 5 is suggested as a negative parity band as that of band 4. A sample spectrum is provided in Fig. 2(c).

Band 6 is a new band deduced from the present work, which decays predominantly to low-lying states by four new linking transitions, and consequently the excitation energies of band 6 are fixed. Multipolarity analysis indicates that the 883 keV linking transition is of $\Delta I = 2$ character with DCO

ratios of 0.95 obtained by gating on the quadrupole transition and the 921, 1052, 432 keV linking transitions are of $\Delta I = 1$ character. Considering the multipolarity of the linking transitions, the spin-parity assignment of the lowest observed state of band 6 is confirmed. Four new intraband transitions of 185, 269, 257, 408 keV are observed. Multipolarity analysis indicates that the intraband transitions have dipole character, and the spin of this band is extended to $I^\pi = (15^+)$. In addition, the linking transitions of 293 and 272 keV between bands 6 and 7 are established for the first time. A sample γ - γ coincidence spectrum supporting the level scheme of band 6 is shown in Fig. 2(d).

IV. DISCUSSION

Band 4 is a new $\Delta I = 2$ band with an $I^\pi = (10^-)$ band-head feeding into the band 1 with the configuration of $\pi g_{9/2}^{-1} \otimes \nu h_{11/2}$. The decoupled band 4 has a large signature splitting, therefore, the proton is likely to occupy a high- j and low- Ω orbital of $d_{5/2}$, $g_{7/2}$, or $h_{11/2}$ by one-particle-one-hole proton excitation over the $Z = 50$ gap, leaving a pair of $g_{9/2}$ proton holes. In fact, $\pi g_{7/2}$ and $\pi d_{5/2}$ $\Delta I = 2$ bands have been

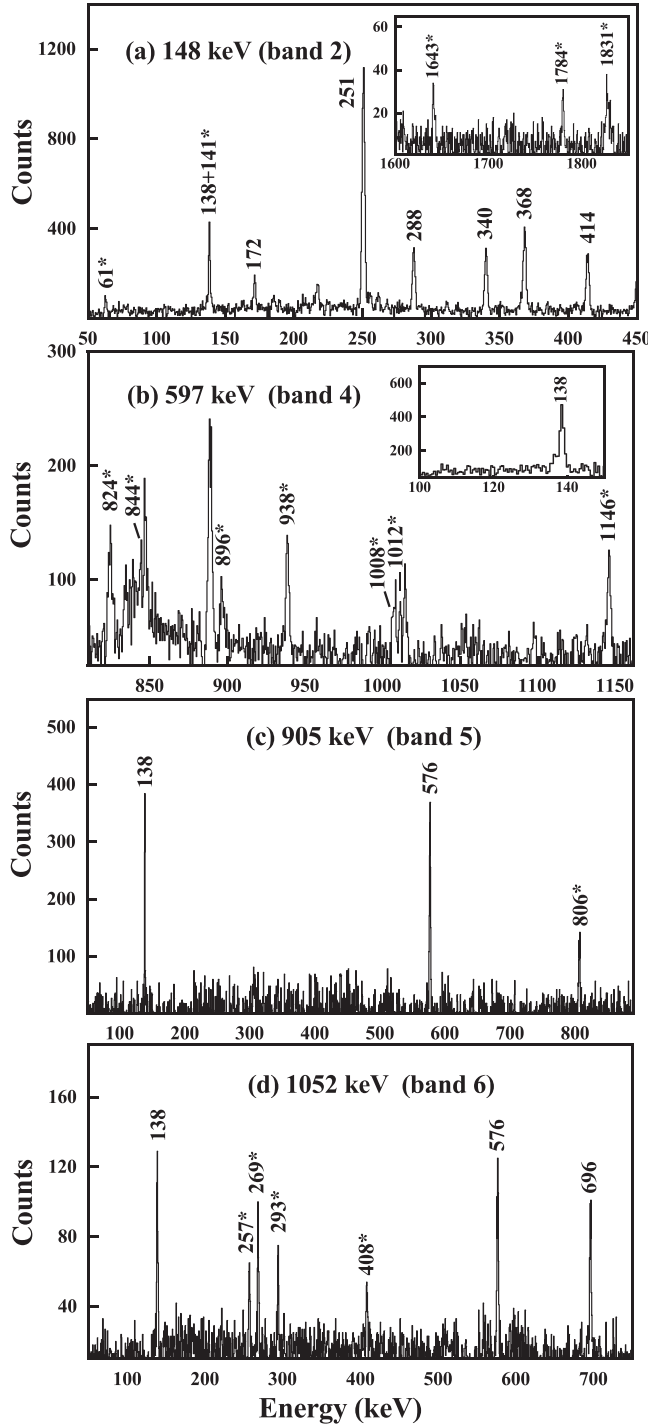


FIG. 2. γ -ray coincidence spectra with gates set on the (a) 148 keV, (b) 597 keV, (c) 905 keV, and (d) 1052 keV. The newly identified γ rays are marked with the asterisks.

reported in ^{110}In and ^{112}In [15,16], whereas the band based on a $\pi h_{11/2}$ orbital is not observed in odd-odd In isotopes, because proton $g_{7/2}$ and $d_{5/2}$ are energetically favored over $h_{11/2}$ at low rotational frequencies. Additionally, band 4 has a negative parity. Hence, the configuration of band 4 is tentatively suggested to $\pi g_{9/2}^{-2}d_{5/2} \otimes \nu h_{11/2}$. To further interpret this structure, the spins I of band 4 in ^{114}In and the $\Delta I = 2$

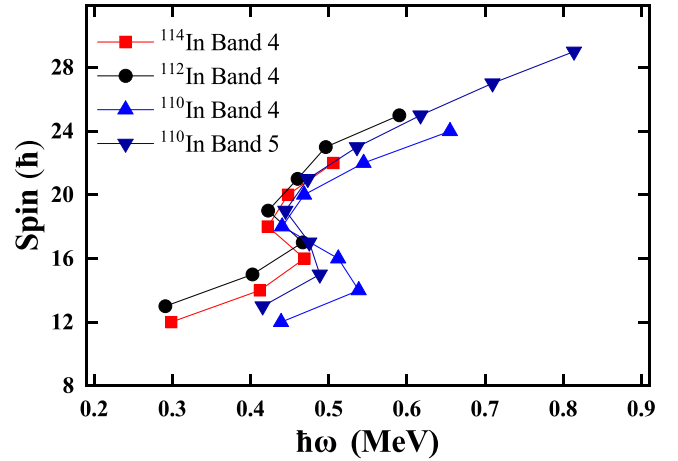


FIG. 3. Experimental spins as a function of rotational frequency for band 4 in $^{110,112,114}\text{In}$ and band 5 in ^{110}In [15,16].

bands of isotopes ^{110}In and ^{112}In are plotted in Fig. 3 as a function of rotational frequency ω , where $\hbar\omega(I) = [E(I) - E(I - 2)]/2$. In Fig. 3, it is clear that these bands exhibit very similar behavior, including the frequencies of the observed alignments and the corresponding gains in spin. Moreover, the similar bands in ^{110}In and ^{112}In were previously interpreted as being based on the configuration $\pi g_{9/2}^{-2}d_{5/2} \otimes \nu h_{11/2}$, with the observed large backbend attribute to the alignment of the two $h_{11/2}$ neutrons. In the present work, a sharp backbend in band 4 is also observed around $\hbar\omega \approx 0.46$ MeV. Therefore, we suggest that band 4 of ^{114}In have a four-quasiparticle $\pi g_{9/2}^{-2}d_{5/2} \otimes \nu h_{11/2}$ configuration before the backbend and a six-quasiparticle $\pi g_{9/2}^{-2}d_{5/2} \otimes \nu h_{11/2}^3$ configuration after the backbend.

To further investigate the corresponding rotation mechanism and confirm the configuration assignment of the negative-parity band 4, the classical particle-rotor model (PRM) is applied [22–24]. So far, the classical PRM has been applied successfully to describe the antimagnetic rotational bands in ^{101}Pd [25], ^{103}Pd [7], ^{104}Pd [6], ^{105}Pd [7], ^{105}Cd [26], ^{106}Cd [9], ^{107}Cd [10,26], ^{108}Cd [13], ^{109}Cd [26], ^{110}Cd [13], ^{127}Xe [27], ^{144}Dy [28], ^{142}Eu [29], and ^{143}Eu [30]. In Fig. 4(a), the experimental angular momentum as functions of frequency for band 4 is compared with the classical PRM calculations for the proposed $\pi g_{9/2}^{-2}d_{5/2} \otimes \nu h_{11/2}^3$ configuration and the other candidate $\pi g_{9/2}^{-2}h_{11/2} \otimes \nu(g_{7/2}/d_{5/2})h_{11/2}^2$ configuration. As shown in Fig. 4(a), the calculations of the $\pi g_{9/2}^{-2}d_{5/2} \otimes \nu h_{11/2}^3$ configuration are in general agreement with the trend of the experimental angular momentum of band 4 after the backbend, supporting the configuration assignment of band 4.

In the $A \approx 110$ mass region, the high- Ω $g_{9/2}$ proton holes and low- Ω $h_{11/2}$ neutrons are known to play an active role in the antimagnetic rotation [1]. In the present work, these basic conditions for the occurrence of antimagnetic rotation can be met in band 4. And in adjacent isotope $^{108,110,112}\text{In}$, the phenomenon of antimagnetic rotation has been already reported [15,16]. Hence, band 4 in ^{114}In may have a common origin from AMR.

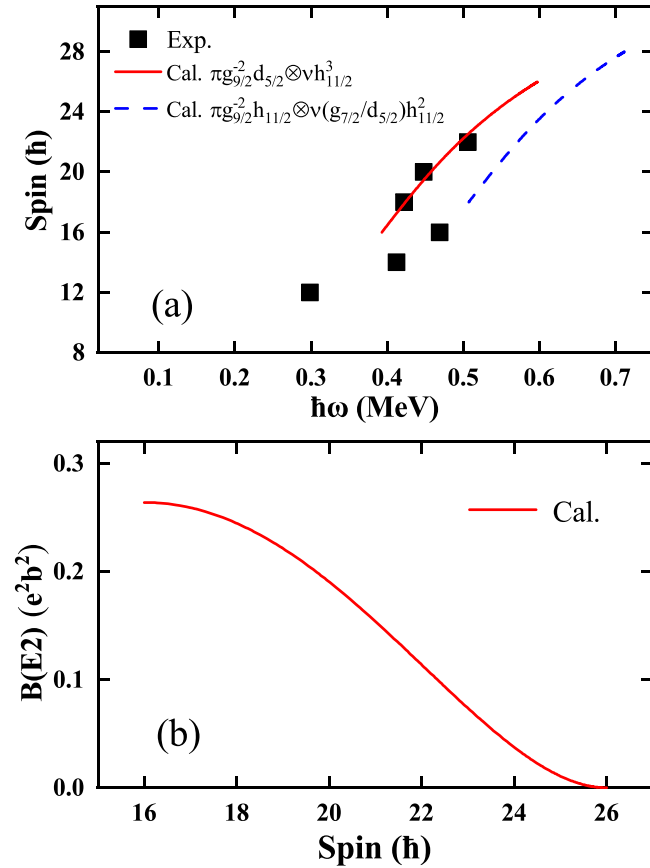


FIG. 4. (a) Spins as a function of the rotational frequency and (b) $B(E2)$ ratios versus spin in the classical PRM calculations for the $\pi g_{9/2}^{-2} d_{5/2} \otimes \nu h_{11/2}^3$ configuration. The experimental values for band 4 are also shown in (a).

In order to examine the possible two-shears-like mechanism in band 4, the angular-momentum components along the axes for the $\pi g_{9/2}^{-2} d_{5/2} \otimes \nu h_{11/2}^3$ configuration after the backbend are presented in Fig. 5. It is clear from Fig. 5 that the two proton hole angular momentum vectors j_h are pointing opposite to each other and nearly perpendicular to the particle angular momentum vector j_p at the bandhead. As the rotational frequency increases, the gradual alignment of the vectors j_h of the two $g_{9/2}$ proton holes toward the vector j_p generates a higher angular momentum, while the direction of the total angular momentum stays unchanged. Therefore, the two shears simultaneously close by moving one blade toward the other. In such a way, the two-shears-like mechanism in ^{114}In is clearly demonstrated in Fig. 5.

Typical characteristics of AMR include weak $E2$ transitions, reflecting the small deformation of the core, and a decreasing tendency of the reduced transition probability $B(E2)$ values with increasing spin, which results in large ratios of the dynamic moments of inertia $\mathfrak{S}^{(2)}$ to the $B(E2)$ values [1,12]. The calculated $B(E2)$ values are shown in the Fig. 4(b). It is interesting to note that the calculated $B(E2)$ values of band 4 decrease smoothly with increasing rotational frequency for the assigned configuration. In addition, the calculated $\mathfrak{S}^{(2)}/B(E2)$ ratios for the configuration above

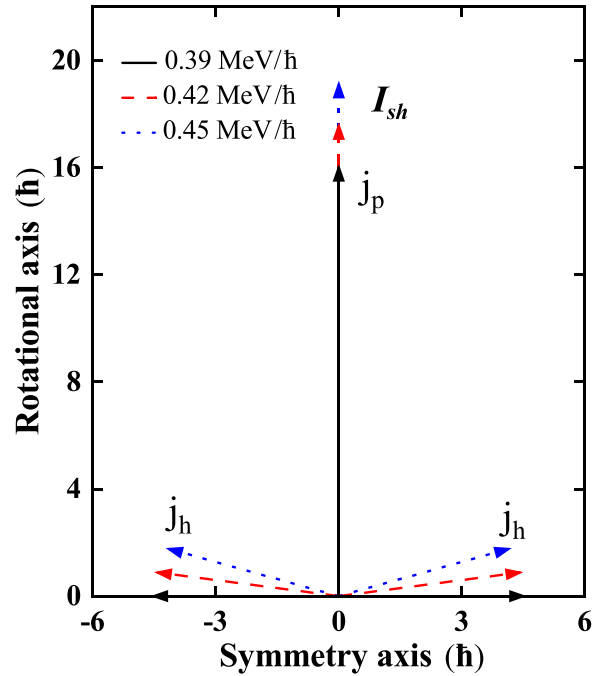


FIG. 5. Angular momentum vectors of neutrons and the proton particle, j_p , and the two high- Ω $g_{9/2}$ proton holes, j_h , at rotational frequencies of 0.39, 0.42, 0.45 MeV/ \hbar .

mentioned are substantial [$> 100\hbar^2\text{MeV}^{-1}(eb)^{-2}$]. These calculated results are consistent with the characteristics of the AMR. However, to confirm this suggestion, the further experimental results of absolute $B(E2)$ transition probabilities based on lifetime measurements are desirable to reach a definitive conclusion.

Band 5, which has negative parity and $\alpha = 1$ signature, is observed for the first time decaying to the yrast band. Considering the Fermi surface for both protons and neutrons of the ^{114}In nucleus, band 5 may be viewed as the $\pi g_{9/2}^{-2} g_{7/2} \otimes \nu h_{11/2}$. Indeed, the similar structures with the same configuration have also been observed in ^{108}In and ^{110}In [15].

The dipole band 6 is a new band, which decaying to the $\pi g_{9/2}^{-1} \otimes \nu (g_{7/2}/d_{5/2}) h_{11/2}^2$ band 2 and low-lying states. As shown in Fig. 1, band 6 has the same positive parity as band 2. The existence linking transitions between bands 6 and 2 indicate that the two bands possibly have similar matrix elements, and the approximate excitation energy among band 2 and band 6 suggests that the band 6 is likely to be built on the same three-quasineutron configuration as that of band 2, since one- or five-quasineutron configurations would not so closely match either the spins or energies observed in both bands. Considering the properties mentioned above, band 6 has been tentatively assigned as $\pi g_{9/2}^{-1} \otimes \nu (g_{7/2}/d_{5/2}) h_{11/2}^2$ configuration, which differ with band 2 only by the favored or unfavored positive-parity neutron orbital. For completeness, the configurations of newly identified bands and previous reported bands [20] for ^{114}In are tabulated in Table II.

Band 1 is a negative parity yrast band with the configuration of $\pi g_{9/2}^{-1} \otimes \nu h_{11/2}$ [20]. The similar yrast bands

TABLE II. Summary of proposed configurations in ^{114}In .

Band	configuration
1 ^{a,c}	$\pi g_{9/2}^{-1} \otimes \nu h_{11/2}$
1 ^{b,c}	$\pi g_{9/2}^{-1} \otimes \nu(g_{7/2}/d_{5/2})^2 h_{11/2}$
2 ^c	$\pi g_{9/2}^{-1} \otimes \nu(g_{7/2}/d_{5/2})^2 h_{11/2}^2$
3 ^c	$\pi g_{9/2}^{-1} \otimes \nu h_{11/2}^3$
4 ^a	$\pi g_{9/2}^{-2} d_{5/2} \otimes \nu h_{11/2}$
4 ^b	$\pi g_{9/2}^{-2} d_{5/2} \otimes \nu h_{11/2}^3$
5	$\pi g_{9/2}^{-2} g_{7/2} \otimes \nu h_{11/2}$
6	$\pi g_{9/2}^{-1} \otimes \nu(g_{7/2}/d_{5/2})_{uf} h_{11/2}^2$
7 ^c	$\pi g_{9/2}^{-1} \otimes \nu(g_{7/2}/d_{5/2})^2 (h_{11/2})_{uf}$

^aBefore backbend.

^bAfter backbend.

^cThe configurations adopted from prior work [20].

based on the same $\pi g_{9/2}^{-1} \otimes \nu h_{11/2}$ configuration have also been identified in neighboring In isotope $^{104,106,108,110,112}\text{In}$ [15,16,31] and Ag isotope $^{102,104,106,108,110}\text{Ag}$ [32–36]. For comparison, the excitation energies of the yrast bands in $^{104,106,108,110,112,114}\text{In}$ and $^{102,104,106,108,110}\text{Ag}$ are presented in Fig. 6. One can see from Fig. 6, as the neutron number increases, most of the levels of the yrast bands lowers in excitation energy. It indicates that the neutron Fermi level is going up into the $N = 4$ shell towards the $\nu h_{11/2}$ subshell with increasing neutron number.

V. SUMMARY

Level structures of ^{114}In have been studied through the $^{110}\text{Pd} (^7\text{Li}, 3n)^{114}\text{In}$ reaction. The previously established level scheme of ^{114}In has been extended by the addition of more than 30 new transitions. A new $\Delta I = 2$ band has been observed for the first time. The configuration of this band is assigned to $\pi g_{9/2}^{-2} d_{5/2} \otimes \nu h_{11/2}$ before the backbend and $\pi g_{9/2}^{-2} d_{5/2} \otimes \nu h_{11/2}^3$ after the backbend. Based on the classical particle-rotor model calculations, the properties of the $\Delta I = 2$ band after the backbend show general agreement with the characteristics of two-shears-like mechanism. Thus, the structure is suggest to be the candidate antimagnetic rotational band in ^{114}In . However, to confirm this suggestion, the further experimental results of absolute $B(E2)$ transition probabilities based on lifetime measurements are desirable. Besides, two new bands and a cascade have also been observed, among which the configuration of the short band is tentatively

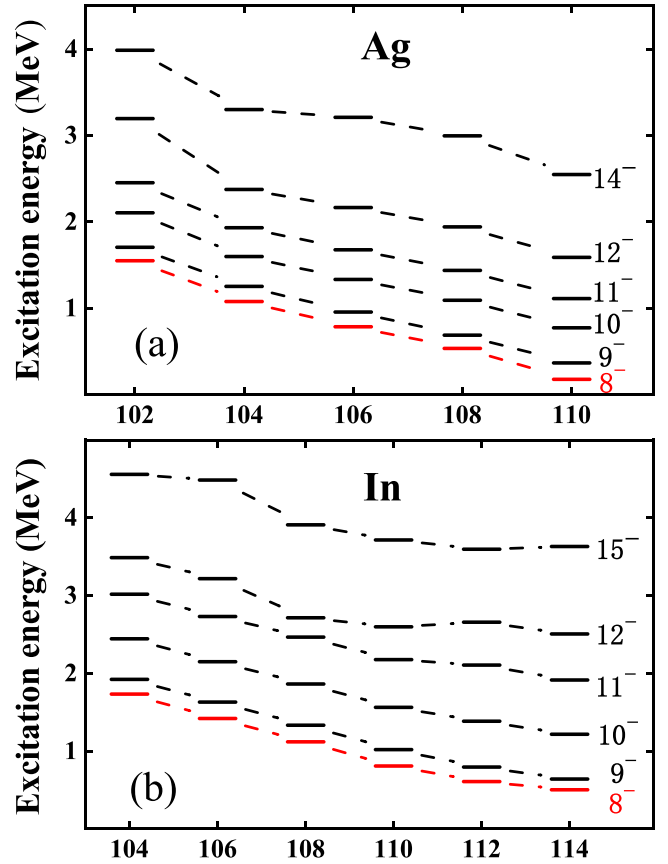


FIG. 6. The excitation energy of the yrast band for (a) $^{102,104,106,108,110}\text{Ag}$ and (b) $^{104,106,108,110,112,114}\text{In}$.

suggested to $\pi g_{9/2}^{-2} g_{7/2} \otimes \nu h_{11/2}$. And a new positive-parity $\Delta I = 1$ band build on the $\pi g_{9/2}^{-1} \otimes \nu(g_{7/2}/d_{5/2}) h_{11/2}^2$ is identified.

ACKNOWLEDGMENTS

This work is supported by the National Nature Science Foundation of China (11975315, U1867210, U1932209, U2167201, U2167202, 12175086), Jilin Scientific and Technological Development Program (20230101009JC), Science and Technology Research Planning Project of Jilin Provincial Department of Education (JJKH20220965KJ), Natural Science Foundation of Chongqing, China (CSTB2022NSCQ-MSX0315), Natural Science Foundation of Sichuan China (23NSFSC1051), and Graduate Innovation Fund of Jilin University (2022239).

[1] S. Frauendorf, *Rev. Mod. Phys.* **73**, 463 (2001).
 [2] S. Sihotra, *Int. J. Mod. Phys. E* **31**, 2250020 (2022).
 [3] S. Sihotra, D. Kumar, M. Kaur, V. Singh, S. Saha, J. Sethi, R. Palit, N. Singh, and D. Mehta, *Phys. Rev. C* **102**, 034321 (2020).
 [4] M. Sugawara, T. Hayakawa, M. Oshima, Y. Toh, A. Osa, M. Matsuda, T. Shizuma, Y. Hatsukawa, H. Kusakari *et al.*, *Phys. Rev. C* **92**, 024309 (2015).

[5] H. Jia, B. Qi, C. Liu, Q. Hu, and S. Y. Wang, *Phys. Rev. C* **97**, 024335 (2018).
 [6] N. Rather, S. Roy, P. Datta, S. Chattopadhyay, A. Goswami, S. Nag, R. Palit, S. Pal, S. Saha *et al.*, *Phys. Rev. C* **89**, 061303(R) (2014).
 [7] Y. K. Pan, K. Y. Ma, and J. B. Lu, *Chin. Phys. C* **46**, 094001 (2022).

- [8] D. Choudhury, A. K. Jain, M. Patial, N. Gupta, P. Arumugam, A. Dhal, R. K. Sinha, L. Chaturvedi, P. K. Joshi *et al.*, *Phys. Rev. C* **82**, 061308(R) (2010); S. Roy and S. Chattopadhyay, *ibid.* **87**, 059801 (2013).
- [9] A. J. Simons, R. Wadsworth, D. G. Jenkins, R. M. Clark, M. Cromaz, M. A. Deleplanque, R. M. Diamond, P. Fallon, G. J. Lane *et al.*, *Phys. Rev. Lett.* **91**, 162501 (2003).
- [10] D. Choudhury, A. K. Jain, G. A. Kumar, S. Kumar, S. Singh, P. Singh, M. Sainath, T. Trivedi, J. Sethi, S. Saha, S. K. Jadav, B. S. Naidu, R. Palit, H. C. Jain, L. Chaturvedi, and S. C. Pancholi, *Phys. Rev. C* **87**, 034304 (2013).
- [11] A. J. Simons, R. Wadsworth, D. G. Jenkins, R. M. Clark, M. Cromaz, M. A. Deleplanque, R. M. Diamond, P. Fallon, G. J. Lane *et al.*, *Phys. Rev. C* **72**, 024318 (2005).
- [12] P. Datta, S. Chattopadhyay, S. Bhattacharya, T. K. Ghosh, A. Goswami, S. Pal, M. Saha Sarkar, H. C. Jain, P. K. Joshi *et al.*, *Phys. Rev. C* **71**, 041305(R) (2005).
- [13] S. Roy, S. Chattopadhyay, P. Datta, S. Pal, S. Bhattacharya, R. K. Bhowmik, A. Goswami, H. C. Jain, R. Kumar *et al.*, *Phys. Lett. B* **694**, 322 (2011).
- [14] C. Majumder, H. P. Sharma, S. Chakraborty, and S. S. Tiwary, *Int. J. Mod. Phys. E* **27**, 1850034 (2018).
- [15] C. J. Chiara, D. B. Fossan, V. P. Janzen, T. Koike, D. R. LaFosse, G. J. Lane, S. M. Mullins, E. S. Paul, D. C. Radford *et al.*, *Phys. Rev. C* **64**, 054314 (2001).
- [16] X. W. Li, J. Li, J. B. Lu, K. Y. Ma, Y. H. Wu, L. H. Zhu, C. Y. He, X. Q. Li, Y. Zheng *et al.*, *Phys. Rev. C* **86**, 057305 (2012).
- [17] K. Y. Ma, J. B. Lu, J. Li, D. Yang, Y. J. Ma, W. J. Sun, X. Guan, D. M. Zhang, L. H. Zhu *et al.*, *Phys. Rev. C* **100**, 014326 (2019).
- [18] M. Wang, W. J. Sun, B. H. Sun, J. Li, L. H. Zhu, Y. Zheng, G. L. Zhang, L. C. He, W. W. Qu *et al.*, *Eur. Phys. J. A* **56**, 31 (2020).
- [19] K. S. Krane, R. M. Steffen, and R. M. Wheeler, *Nucl. Data Tables* **11**, 351 (1973).
- [20] C. B. Li, Y. Zheng, X. G. Wu, X. F. Li, C. Y. He, G. S. Li, S. H. Yao, B. B. Yu, X. P. Cao *et al.*, *Eur. Phys. J. A* **47**, 141 (2011).
- [21] J. Blachot, *Nucl. Data Sheets* **97**, 593 (2002).
- [22] A. Bohr and B. Mottelson, *Nuclear Structure*, Vol. 2 (Benjamin, New York, 1975).
- [23] R. M. Clark and A. O. Macchiavelli, *Annu. Rev. Nucl. Part. Sci.* **50**, 1 (2000).
- [24] A. O. Macchiavelli, R. M. Clark, M. A. Deleplanque, R. M. Diamond, P. Fallon, I. Y. Lee, F. S. Stephens, and K. Vetter, *Phys. Lett. B* **450**, 1 (1999).
- [25] V. Singh, S. Sihotra, S. Roy, M. Kaur, S. Saha, J. Sethi, R. Palit, N. Singh, S. S. Malik *et al.*, *J. Phys. G: Nucl. Part. Phys.* **44**, 075105 (2017).
- [26] S. Roy and S. Chattopadhyay, *Phys. Rev. C* **83**, 024305 (2011).
- [27] S. Chakraborty, H. P. Sharma, S. S. Tiwary, C. Majumder, P. Banerjee, S. Ganguly, S. Rai, Pragati, S. Muralithar *et al.*, *J. Phys. G: Nucl. Part. Phys.* **47**, 015103 (2020).
- [28] M. Sugawara, Y. Toh, M. Oshima, M. Koizumi, A. Osa, A. Kimura, Y. Hatsukawa, J. Goto, H. Kusakari *et al.*, *Phys. Rev. C* **79**, 064321 (2009).
- [29] S. Ali, S. Rajbanshi, B. Das, S. Chattopadhyay, M. Saha Sarkar, A. Goswami, R. Raut, A. Bisoi, S. Nag, S. Saha, J. Sethi, R. Palit, G. Gangopadhyay, T. Bhattacharjee, S. Bhattacharyya, G. Mukherjee, A. K. Singh, and T. Trivedi, *Phys. Rev. C* **96**, 021304(R) (2017).
- [30] S. Rajbanshi, S. Roy, S. Nag, A. Bisoi, S. Saha, J. Sethi, T. Bhattacharjee, S. Bhattacharyya, S. Chattopadhyay *et al.*, *Phys. Lett. B* **748**, 387 (2015).
- [31] D. Seweryniak, J. Kownacki, L.-O. Norlin, C. Fahlander, A. Atac, J. Blomqvist, B. Cederwall, H. Grawe, A. Johnson *et al.*, *Nucl. Phys. A* **589**, 175 (1995).
- [32] S. Rastikerdar, *Yad. Fiz.* **64**, 1285 (2001) [*Phys. At. Nucl.* **64**, 1210 (2001)].
- [33] Z. G. Wang, M. L. Liu, Y. H. Zhang, X. H. Zhou, B. T. Hu, N. T. Zhang, S. Guo, B. Ding, Y. D. Fang *et al.*, *Phys. Rev. C* **88**, 024306 (2013).
- [34] P. Joshi, M. P. Carpenter, D. B. Fossan, T. Koike, E. S. Paul, G. Rainovski, K. Starosta, C. Vaman, and R. Wadsworth, *Phys. Rev. Lett.* **98**, 102501 (2007).
- [35] C. Liu, S. Y. Wang, B. Qi, D. P. Sun, S. Wang, C. J. Xu, L. Liu, P. Zhang, Z. Q. Li *et al.*, *Phys. Rev. C* **88**, 037301 (2013).
- [36] K. Y. Ma, H. Wang, H. N. Pan, J. B. Lu, Y. J. Ma, D. Yang, Q. Y. Yang, X. Guan, J. Q. Wang *et al.*, *Phys. Rev. C* **103**, 024302 (2021).